J Appl Electrochem (2012) 42:1057–1064
DOI 10.1007/s10800-012-0482-5

ORIGINAL PAPER

Effects of VGCF pretreatment on the characteristics of Fe_2O_3/VGCF composites as anode materials for Li-ion batteries

Sang-Wook Han · Dong-Won Jung · Jae-Hun Jeong · Eun-Suok Oh

Received: 3 July 2012 / Accepted: 17 September 2012 / Published online: 27 September 2012

Abstract Two main topics were handled in this study: loss minimization in the irreversible capacity of vapor-grown carbon fibers (VGCFs) by pretreatment techniques and reversible capacity increase in pretreated VGCFs by the deposition of nano-sized Fe_2O_3. VGCFs were ball-milled and acid-treated, and nano-sized Fe_2O_3 particles were supported on the pretreated VGCFs. Their performance as anodes in lithium-ion batteries was characterized using a variety of techniques. Compared to the electrode containing pristine VGCF only, electrodes composed of the pretreated-VGCFs enhanced both charge transfer and discharge capacities due to an increase in lithium-ion mobility. Moreover, the Fe_2O_3 nanoparticles supported on the pretreated VGCFs could eliminate defects and functional groups on the surface of VGCFs generated by the pretreatment, such that the composite of Fe_2O_3 and pretreated VGCF showed higher reversible capacity at any rate of charge/discharge than the composite of Fe_2O_3 and the pristine VGCF. Therefore, the Fe_2O_3/pretreated VGCF composites could be a good candidate for high capacity anodes.

Keywords Lithium ion battery · Anode active materials · Vapor-grown carbon fiber (VGCF) · Hematite · Functional groups

1 Introduction

Graphite is commercially used as an active anode material in lithium-ion batteries (LIBs) due to its stable structure, high conductivity, and low cost. Since LIBs are being faced with increasing specific energy and power densities in accordance with the development of electric vehicles and energy storage devices, future competitive anode materials are required to overcome the limited capacity of graphite (372 mAh g^{-1}), to possess electrochemical stability, and to be relatively low cost [1–3].

Recent studies [4–6] proved that iron oxides could be a good choice for anode materials due to their high lithium-ion storage as well as natural abundance. Iron oxides exist in the form of either hematite (Fe_2O_3) or magnetite (Fe_3O_4) in nature and react with lithium ions as follows [4, 7, 8];

$$Fe_2O_3 + 6Li^+ + 6e^- \rightleftarrows 2Fe + 3Li_2O \quad (1)$$

$$Fe_3O_4 + 8Li^+ + 8e^- \rightleftarrows 3Fe + 4Li_2O \quad (2)$$

The theoretical capacities of Fe_2O_3 and Fe_3O_4 are approximately 1,004 and 924 mAh g^{-1}, respectively [7, 8], which are approximately 2.5 times as large as that of graphite. However, most transition metal oxides undergo significant volume change during the charge and discharge processes. For instance, the volume expansion of CuO and Co_3O_4 was more than 100 % and iron oxides experienced equivalent problems [7–10]. This expansion generates mechanical stresses in the electrode, which lead to electrical insulation by the formation of cracks and delamination of active materials from the current collector. Ultimately, the significant volume change results in severe capacity fading. Various approaches to enhance the cycle ability of transition metal oxides have been carried out. One crucial attempt was to disperse nano-sized metal oxide particles on a stable matrix such as graphite [11, 12], graphene [13, 14], or carbon nanotubes (CNTs) [15, 16].

Carbon fiber, especially vapor-grown carbon fiber (VGCF), could also be used for a stable matrix of iron

S.-W. Han · D.-W. Jung · J.-H. Jeong · E.-S. Oh (✉)
School of Chemical Engineering & Bioengineering, University of Ulsan, Ulsan 680-749, Republic of Korea
e-mail: esoh1@ulsan.ac.kr

oxides due to its good electrochemical durability, excellent electrical conductivity, and low cost in comparison with CNT or grapheme [17]. Despite the high capacity of iron oxides, a significant capacity loss occurred in the course of use owing to the structural characteristics of VGCF. Use of VGCF as an active material has also been investigated by several researchers [18–20], while conventional electrodes used primarily a small amount of VGCF as a conducting agent. They reported a significant initial irreversible capacity resulting from the high aspect ratio of VGCF. The long pathway for lithium ions intercalation/deintercalation acted as a resistance to the movement of lithium ions so that the irreversible capacity increased. In this study, we focus on minimizing the irreversible capacity loss of VGCF by ball-milling and acid-treatments, and we additionally deposit Fe_2O_3 nanoparticles on the pretreated VGCF to increase the reversible capacity of the anode. A variety of characterization techniques will be applied to investigate the possibility of Fe_2O_3/pretreated VGCF composites as anode materials.

2 Experimental

VGCF (Grasker^{TM}, Nikkiso Co., 5 g) along with steel beads was placed in a SKD-61 steel jar and was ball-milled for 6 h to decrease the aspect ratio of the VGCF. This will be denoted as VGCF-a. Subsequently, the VGCF-a was ultrasonically dispersed and stirred for 1 h with a mixture of 4 M H_2SO_4 and 4 M H_2O_2. It was then washed with deionized water and ethanol, and dried in a vacuum oven at 80 °C. Finally, it was heat-treated at 900 °C in a N_2 atmosphere for 1 h, and this sample will be denoted as VGCF-b in what follows.

Each VGCF, including pristine VGCF, was added to 300 ml of ethylene glycol (EG) and was ultrasonically dispersed for 1 h. $FeCl_3{\cdot}6H_2O$ (Kanto Chem. Co.) as a precursor of iron oxides was dissolved in 30 ml of EG, and was mixed with the EG solution containing the VGCFs. This solution was then heated to 190 °C. Then, 1 M NaOH was added drop-wise to the solution so as to adjust to pH 10–11, and the solution was maintained in these conditions for 3 h to well disperse iron particles on VGCFs. The composite was washed with deionized water and ethanol, and dried overnight in a vacuum oven at 80 °C. Finally, the dried samples were heat-treated at 350 °C in an air atmosphere for 5 h to form metal oxides on the surface of VGCFs. These are referred to as Fe_2O_3/VGCF, Fe_2O_3/VGCF-a, and Fe_2O_3/VGCF-b, depending upon the VGCF used in the process.

An X-ray diffractometer (XRD, Rigaku, RAD-3C) was used to characterize the crystal structures of both VGCFs and Fe_2O_3/VGCFs. The weight percentage of iron oxide in the composites was measured using a thermogravimetric analyzer (TGA, TA instrument, Q50), and their particle sizes and morphologies were observed by field emission scanning electron microscopy (Carl Zeiss, Supra40) and transmission electron microscopy (TEM, Jeol, JEM-2010, 2100F). Fourier transform infrared (FT-IR, Nicolet IR 200, Thermo Scientific) spectra were also analyzed to investigate change in functional groups on the samples.

To evaluate the electrochemical properties of the samples, CR2016 coin cells with lithium metal as a reference electrode were assembled in an argon-filled glove box. The working electrodes were made up of 60 wt% of VGCFs or Fe_2O_3/VGCFs, 25 wt% ketjen black and 15 wt% polyvinylidene fluoride (Solef 5130, Belgium) as a binder. The electrolyte used in the cells was 1 M $LiPF_6$ (Panaxetec Co.) in a 1:1:1 mixture of ethylene carbonate, ethylmethyl carbonate, and dimethyl carbonate. The coin cells were galvanostatically charged to 3 V and discharged to 5 mV with various current densities in a battery test system (PNE solution, BCP50. 1-32). Furthermore, the electrochemical oxidation/reduction characteristics of the active materials were evaluated using cyclic voltammetry (CV, Biologis, VSP) performed at a scan rate of 0.5 mV/s, and electrochemical impedance spectroscopy (EIS) tests were also conducted at a frequency range of 0.01 Hz to 100 kHz.

3 Results and discussion

The structural evolutions of VGCFs and Fe_2O_3/VGCFs were characterized by XRD and their results are displayed in Fig. 1. The XRD patterns of VGCFs show the $P6_3mc$ space group and hexagonal crystal structures (JCPDS no. 75-1621). Based on the observation that the diffraction peak intensities of pretreated VGCFs corresponding to (002) and (004) crystal plans are lower than those of pristine VGCF, the pretreatment of VGCF increases the full width at half maximum, decreases the length of the VGCF, and reduces the degree of crystallization due to the formation of defects on the surface. However, the peaks appear at the same locations, indicating no change in *d*-spacing even after ball-milling and acid-treatment. The XRD patterns of Fe_2O_3/VGCFs shown in Fig. 1b indicate the $R\bar{3}c$ space group and rhombohedral crystal structures of the Fe_2O_3 (JCPDS no. 87-1164). In addition, according to the Scherrer's equation [21], the average particle sizes of the Fe_2O_3 distributed on VGCF, VGCF-a, and VGCF-b are 10, 18, and 24 nm, respectively. The ball-milling and acid-treatment may form defects and functional groups on the surface of VGCF, inducing much adsorption of iron ions, and consequently, the formation of numerous nuclei at the sites increases particle sizes.

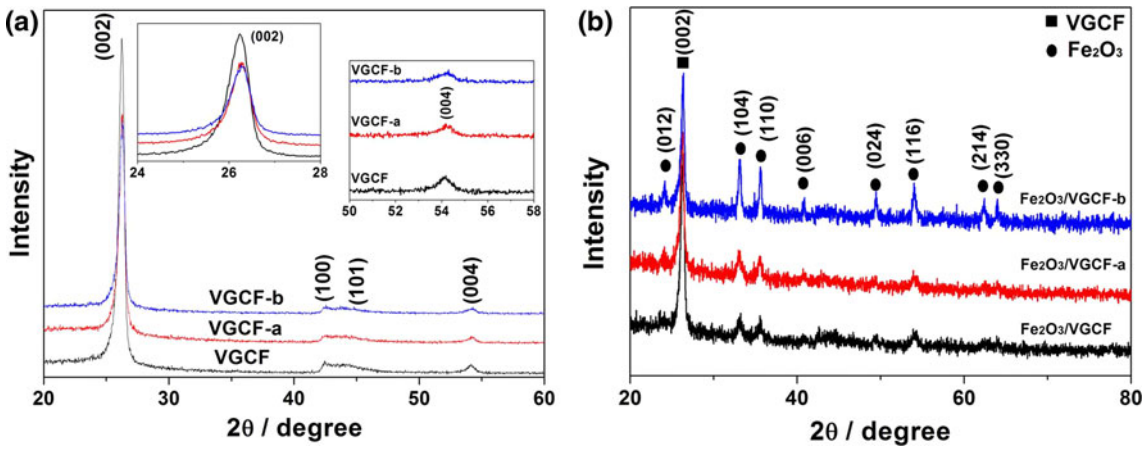

Fig. 1 XRD patterns of **a** VGCFs and **b** Fe_2O_3/VGCFs

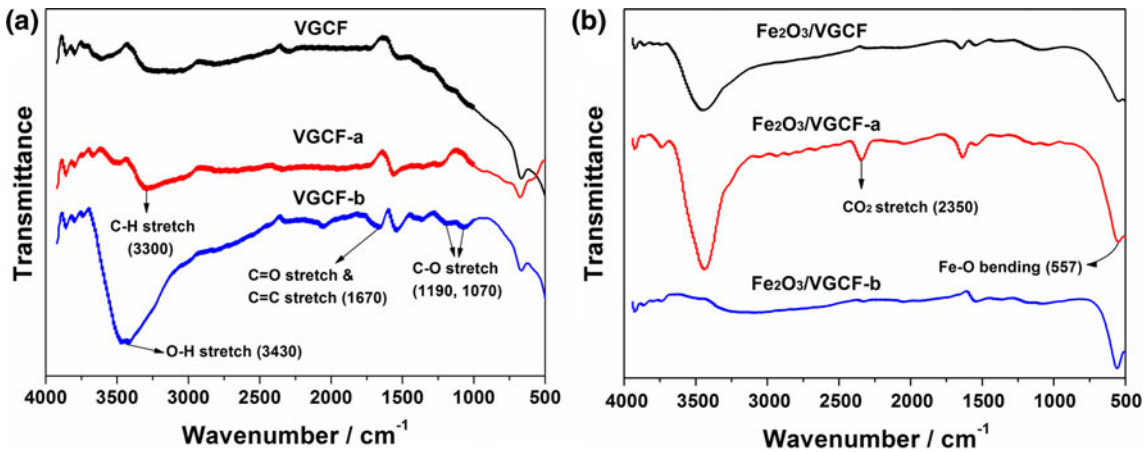

Fig. 2 FT-IR spectra of **a** VGCFs and **b** Fe_2O_3/VGCFs

This formation of functional groups was confirmed by FT-IR measurements, as shown in Fig. 2a. The FT-IR spectra of VGCF and VGCF-a showed only weak peaks, including a broad peak of the VGCF-a sample at 3,300 cm^{-1}, attributed to a C–H stretch. In contrast, the FT-IR spectrum of VGCF-b exhibits several peaks at 3430, 1670, 1190, and 1070 cm^{-1} corresponding to O–H stretch, C=O and C=C stretches, epoxy C–O stretch, and alkoxy C–O stretch, respectively [22–24]. In particular, the strong O–H stretch peak indicates that a significant amount of carboxyl groups were formed at the defects of VGCF, corresponding to the C–H stretch after the VGCF was acid-treated. FT-IR analysis of Fe_2O_3/VGCF-b shown in Fig. 2b displays no apparent peaks except for a Fe–O stretch appearing at 557 cm^{-1} [25]. From this, it is concluded that most iron oxides were anchored and nucleated at the sites of functional groups. However, the Fe_2O_3/VGCF and Fe_2O_3/VGCF-a composites exhibit O–H stretch, indicating that the anchoring process also generates some functional groups on pristine VGCF or ball-milled VGCF.

Figure 3 shows morphologies of VGCF and Fe_2O_3/VGCFs. SEM analysis of pristine VGCF in Fig. 3a shows a typical onion skin structure with an exfoliated graphene layer at some wall surface. From the SEM observation of Fe_2O_3/VGCF-a displayed in Fig. 3b, VGCF nodes noted as dotted circles in the lower inset appear in ball-milled VGCF. The node was examined closely using TEM, as shown in Fig. 3c. In the dotted circle, mechanical twin bends can be observed. These are attributed to a rapid change in the grain orientation between twin boundaries by continuous shearing force. This shearing force during ball-milling also peels off outer layers of VGCF to form a thin layer of graphite, providing a support for Fe_2O_3 particles. Further, a large amount of agglomerated Fe_2O_3 particles was also observed, as shown in the upper inset of Fig. 3b. It is clear from Fig. 3d that such agglomerated particles were reduced when Fe_2O_3 particles were formed on the surface of balled-milled and acid-treated VGCF. In addition, numerous Fe_2O_3 nanoparticles are well distributed on the surface of the pretreated VGCF, as seen in the inset of

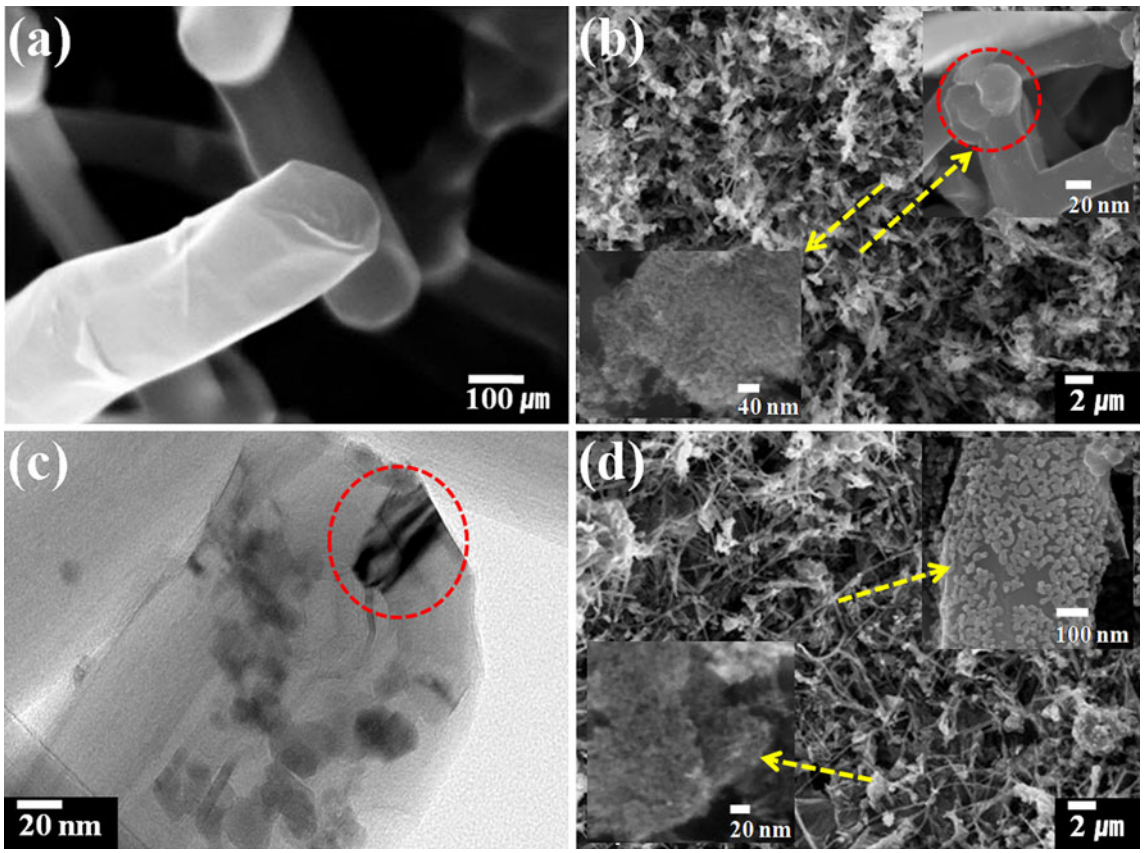

Fig. 3 SEM images of **a** pristine VGCF and **b** Fe_2O_3/VGCF-a, **c** TEM image of Fe_2O_3/VGCF-a, and **d** SEM image of Fe_2O_3/VGCF-b

Fig. 3d. These well dispersed Fe_2O_3 nanoparticles may contribute to improving the electrical network in the electrodes.

From the TGA analysis shown in Fig. 4, the weight percentages of Fe_2O_3 with respect to VGCF, VGCF-a, or VGCF-b in the composites are approximately 13, 14, and 18 wt%, respectively. As mentioned in previous FT-IR and SEM analyses, the ball-milled and acid-treated VGCF forms more surface and functional groups providing sites for the adsorption of iron ions or nucleation. This leads to higher quantities of Fe_2O_3 in Fe_2O_3/VGCF-b in comparison with Fe_2O_3/VGCF and Fe_2O_3/VGCF-a.

To evaluate the electrochemical characteristics of these materials, coin-half cells were fabricated, and CV, EIS, and cyclic tests were performed. From the CV results displayed in Fig. 5, the reduction/oxidation peaks appearing at 0 and 0.3 V indicate the intercalation/deintercalation of lithium ions into the graphene layers of VGCFs. A strong irreversible peak in the range of 0.25–0.4 V occurs during the first reduction process due to the formation of a solid electrolyte interface (SEI) by the decomposition of electrolytes. Based on the voltage in Fig. 5a–c, as the VGCF is ball-milled and acid-treated, the voltage is getting close to 0.5 V, corresponding to SEI formation on the surface of

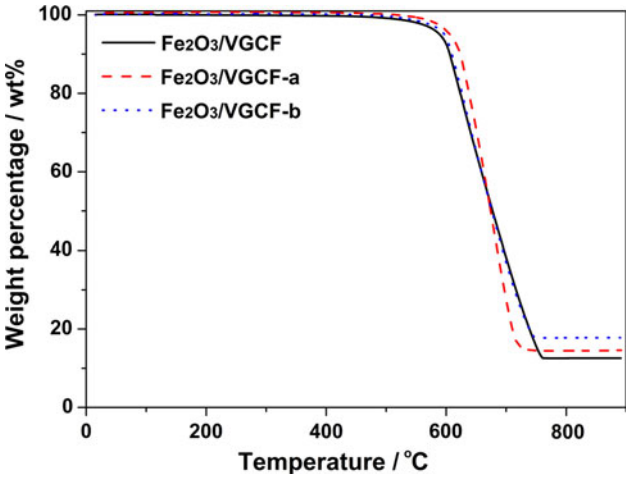

Fig. 4 TGA results for Fe_2O_3/VGCFs composites

typical graphite [22]. Due to the geometrical difference among carbon materials, lithium-ion intercalation into VGCF may be harder than that into graphite so that a larger overpotential is required to generate SEI formation on the surface of VGCF compared to the surface of graphite. This overpotential is decreased with improved diffusion, brought on by shortening the length of VGCF and forming

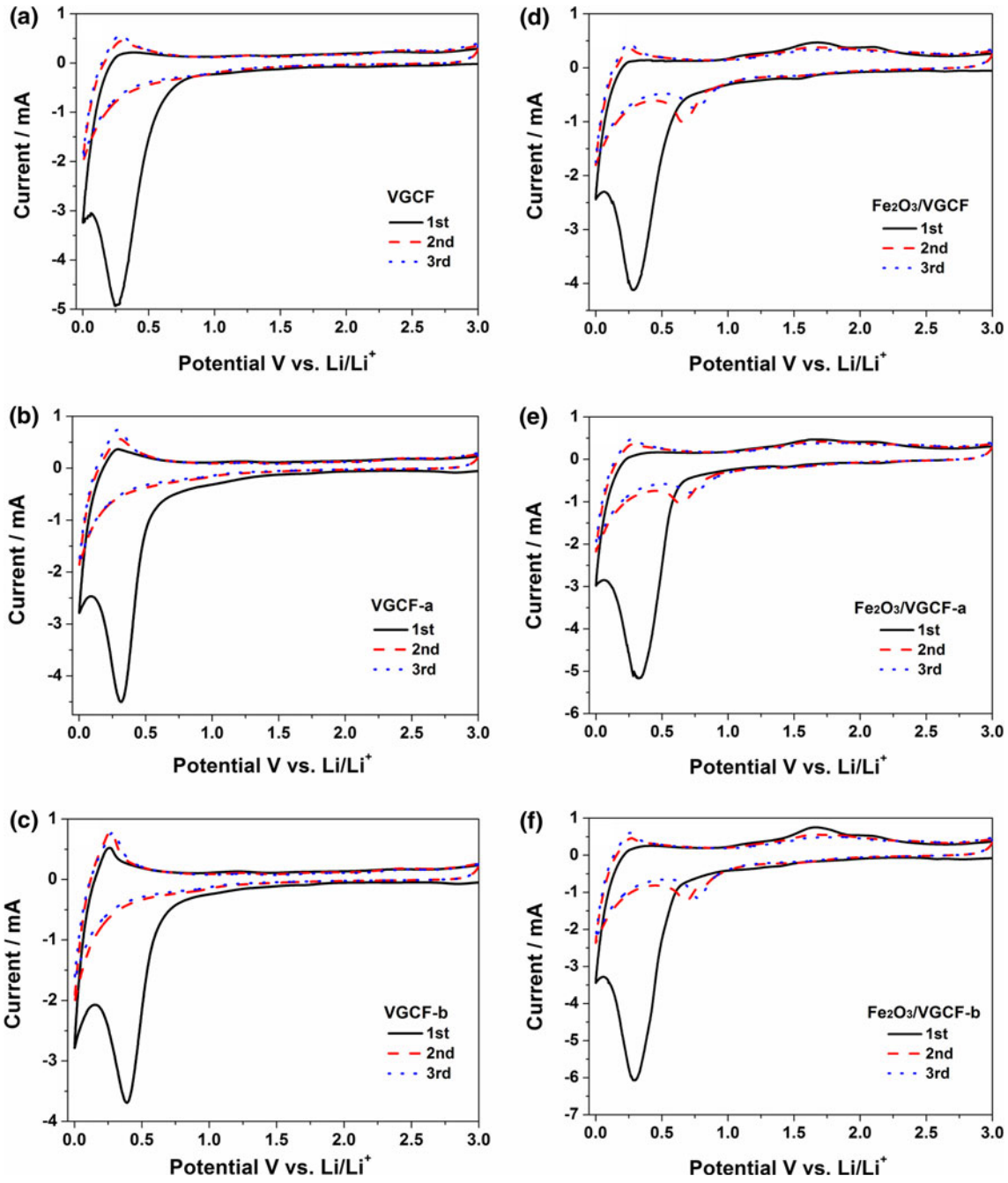

Fig. 5 Cyclic voltammogram of **a** VGCF, **b** VGCF-a, **c** VGCF-b, **d** Fe_2O_3/VGCF, **e** Fe_2O_3/VGCF-a, and **f** Fe_2O_3/VGCF-b electrodes

functional groups on the surface of the VGCF. This is the reason why the voltage attributed to the formation of SEI increases as the pretreatment steps increase.

In the case of Fe_2O_3/VGCFs composites shown in Fig. 5d–f, the following reversible reaction,

$$Fe_2O_3 + 6Li^+ + 6e^- \rightleftarrows 2Fe^0 + 3Li_2O \quad (3)$$

appears around 0.7 V for the reduction of Fe_2O_3 and around 1.7 V for the oxidation of Fe regardless of the composites. Moreover, from the observation that the reduction voltage for the third cycle is higher than that for the second cycle, while the oxidation voltages remains the same, it is clear that the resistance toward the reduction of Fe_2O_3 decreases as the charge/discharge cycles increase in the first few cycles. Kim et al. [26] showed that the charge transfer resistance was gradually reduced in the first 10 cycles of $LiCo_{1/3}Ni_{1/3}Mn_{1/3}$ electrodes due to the aging of electrolyte wetting.

The cyclic performance of the VGCFs and Fe_2O_3/VGCFs composites were evaluated at various current densities, and the results are illustrated in Fig. 6. As seen in

Fig. 6a, the pretreated VGCFs have higher discharge capacity than the pristine VGCF electrode. Ball-milling shortens the length of the VGCF and provides more edge surface for lithium ion intercalation/deintercalation. However, the acid-treated sample after ball-milling, VGCF-b, contains a great number of chemical functional groups on the surface of the VGCF, leading to a loss in reversible capacity [22] compared to the VGCF-a. Even after charging/discharging of 50 cycles, the VGCF, VGCF-a, and VGCF-b samples showed reversible capacities of 470, 556, and 525 mAh g^{-1} at a current density of 100 mA g^{-1}, respectively. The results of the cyclic performance of the Fe_2O_3/VGCF composites are shown in Fig. 6b. These composites showed higher reversible capacities than the VGCF electrodes shown in Fig. 6a due to high capacity iron oxides. Unlike pretreated VGCFs, the Fe_2O_3/VGCF-b sample, the composites of iron oxides and the ball-milled and acid-treated VGCF showed higher reversible capacity than the Fe_2O_3/VGCF-a. In the Fe_2O_3/VGCF-b sample, Fe_2O_3 nanoparticles were anchored at irreversible reactive elements such as surface defects and functional groups on VGCF. The increase in the amount of the deposited Fe_2O_3 nanoparticles and simultaneous decrease in the elements contributes to the increase in the reversible capacity and the electrical network.

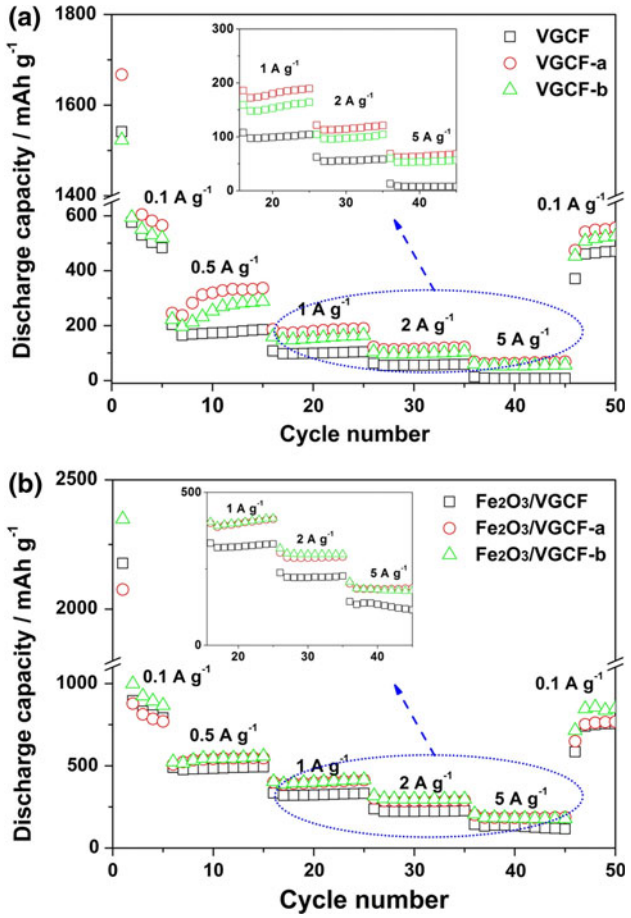

Fig. 6 Cell performance curves at different current densities of **a** VGCF electrodes and **b** Fe_2O_3/VGCF electrodes

Figure 7 illustrates the impedance spectra of the samples after three charge/discharge cycles to see the effect of the pretreatments of VGCF on the resistances of the electrodes. Compared to the pristine VGCF electrode, the pretreated VGCF electrode showed less charge transfer resistance corresponding to the semicircle in the medium frequency region. Connected to the cyclic performance displayed in Fig. 6a, this must be due to easy intercalation/deintercalation by the shortened VGCF via the ball-milling. Yang et al. [27] reported a similar study that the charge transfer resistance increased and the capacity decreased with increase in the length of CNTs as anode materials. Of the pretreated VGCFs, the acid-treated sample, VGCF-b, showed a little higher charge transfer resistance than the sample with no acid-treatment, VGCF-a, due to the existence of functional groups explained above. On the other hand, the charge transfer resistance of the Fe_2O_3/VGCF-b electrode is lower

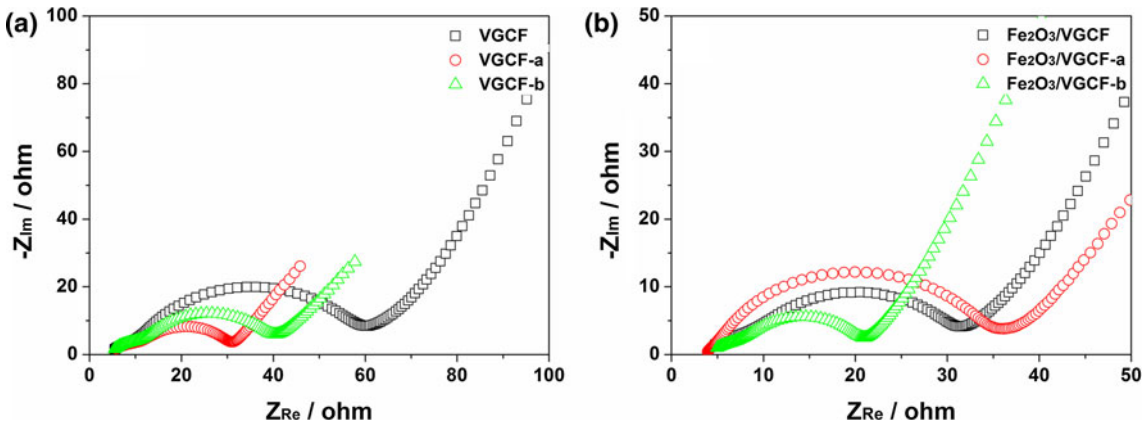

Fig. 7 Nyquist plots of **a** VGCF electrodes and **b** Fe_2O_3/VGCF electrodes

than that of the Fe_2O_3/VGCF-a electrode. These results are consistent with the cyclic performance in Fig. 6b.

Consequently, the dispersion of Fe_2O_3 nanoparticles onto VGCFs can improve the electrical network and reduce the detrimental sites occurring during the pretreatment such as defects and functional groups.

4 Conclusions

Compared to pristine VGCF, ball-milled VGCF, VGCF-a, shortened the fiber length. Additional acid-treatment of VGCF-a to produce VGCF-b formed numerous functional groups on the surface of VGCFs, such as carboxyl and carbonyl groups. Based on electrochemical tests, VGCF-a showed the lowest charge transfer resistance of the three VGCFs due to its shorter length and fewer functional groups, leading to irreversible capacity loss in the course of use. Thus, VGCF-a exhibited a higher capacity of 556 mAh g^{-1} at a current density of 100 mA g^{-1} compared to both the pristine and the acid-treated VGCFs.

The functional groups formed by the acid-treatment provided sites for the adsorption of iron ions or nucleation, and thus led to higher Fe_2O_3 dispersion and a better electrical network on the surface of the VGCF-b, compared to the pristine VGCF and VGCF-a. Consequently, Fe_2O_3/VGCF-b showed lower charge transfer resistance and a higher reversible capacity of 847 mAh g^{-1} than the other two Fe_2O_3/VGCFs. This is a much higher capacity than commercial graphite. In summary, iron oxides that are supported on pretreated VGCFs represent new high capacity anode materials for LIBs.

Acknowledgments The study was supported by the 2012 research fund of the University of Ulsan.

References

1. Cabana J, Monconduit L, Larcher D, Palacín MR (2010) Beyond intercalation-based Li-ion batteries: the state of the art and challenges of electrode materials reacting through conversion reactions. Adv Mater 22:E170–E192
2. Guerfi A, Charest P, Dontigny M, Trottier J, Lagace M, Hovington P, Vijh A, Zaghib K (2011) SiOx—graphite as negative for high energy Li-ion batteries. J Power Sources 196:5667–5673
3. Malini R, Uma U, Sheela T, Ganesan M, Renganathan NG (2009) Conversion reactions: a new pathway to realise energy in lithium-ion battery—review. Ionics 15:301–307
4. Hassan MF, Guo Z, Chen Z, Liu H (2011) Fe_2O_3 as an anode material with capacity rise and high rate capability for lithium-ion batteries. Mater Res Bull 46:858–864
5. Wang G, Liu T, Xie X, Ren Z, Bai J, Wang H (2011) Structure and electrochemical performance of Fe_3O_4/graphene nanocomposite as anode material for lithium-ion batteries. Mater Chem Phys 128:336–340
6. Zhu X, Zhu Y, Murali S, Stoller MD, Ruoff RS (2011) Nanostructured reduced graphene oxide/Fe_2O_3 composite as a high-performance anode material for lithium ion batteries. ACS Nano 5:3333–3338
7. Wang JZ, Zhong C, Wexler D, Idris NH, Wang ZX, Chena LQ, Liu HK (2011) Graphene-encapsulated Fe_3O_4 nanoparticles with 3D laminated structure as superior anode in lithium ion batteries. Chem Eur J 17:661–667
8. Huang Y, Dong Z, Jia D, Guo Z, Cho WI (2011) Preparation and characterization of core-shell structure Fe_3O_4/C nanoparticles with unique stability and high electrochemical performance for lithium-ion battery anode material. Electrochim Acta 56:9233–9239
9. Gao S, Yang S, Shu J, Zhang S, Li Z, Jiang K (2008) Green fabrication of hierarchical CuO hollow micro/nanostructures and enhanced performance as electrode materials for lithium-ion batteries. J Phys Chem C 112:19324–19328
10. Larcher D, Sudant G, Leriche JB, Chabre Y, Tarascon JM (2002) The electrochemical reduction of Co_3O_4 in a lithium cell. J Electrochem Soc 149:A234–A241
11. Jeong JH, Jung DW, Kong BS, Lee JK, Oh ES (2011) Nano-sized Co and Sn–Co alloy/graphite composites for the application of lithium ion batteries. J Ceram Proc Res 12:s105–s109
12. Lin YS, Duh JG, Shieh DT, Yang MH (2010) Effect of pH value on electrochemical property of tin compounds loaded graphite anodes for Li-ion battery applications. J Alloy Compd 490:393–398
13. Lian P, Zhu X, Xiang H, Li Z, Yang W, Wang H (2010) Enhanced cycling performance of Fe_3O_4—graphene nanocomposite as an anode material for lithium-ion batteries. Electrochim Acta 56:834–840
14. Jeong JH, Jung DW, Han SW, Kim KH, Oh ES (2011) Performance of nanosized Fe_3O_4 and CuO supported on graphene as anode materials for lithium ion batteries. J Korean Electrochem Soc 14:239–244
15. Fu Y, Ma R, Shu Y, Cao Z, Ma X (2009) Preparation and characterization of SnO_2/carbon nanotube composite for lithium ion battery applications. Mater Lett 63:1946–1948
16. Ren J, Yang J, Abouimrane A, Wang D, Amine K (2011) SnO_2 nanocrystals deposited on multiwalled carbon nanotubes with superior stability as anode material for Li-ion batteries. J Power Sources 196:8701–8705
17. Hang BT, Doi T, Okada S, Ji Yamaki (2007) Effect of carbonaceous materials on electrochemical properties of nano-sized Fe_2O_3-loaded carbon as a lithium battery negative electrode. J Power Sources 174:493–500
18. Abe H, Murai T, Zaghib K (1999) Vapor-grown carbon fiber anode for cylindrical lithium ion rechargeable batteries. J Power Sources 77:110–115
19. Alcantara R, Lavela P, Ortiz GF, Tirado JL, Stoyanova R, Zhecheva E, Merino C (2004) Nanodispersed iron, tin and antimony in vapour grown carbon fibres for lithium batteries: an EPR and electrochemical study. Carbon 42:2153–2161
20. Endo M, Kim YA, Hayashi T, Nishimura K, Matusita T, Miyashita K, Dresselhaus MS (2001) Vapor-grown carbon fibers (VGCFs): basic properties and their battery applications. Carbon 39:1287–1297
21. Jung DW, Jeong JH, Cha BC, Kim JB, Kong BS, Lee JK, Oh ES (2011) Effects of ball-milled graphite in the synthesis of SnO_2/graphite as an active material in lithium ion batteries. Met Mater Int 17:1021–1026
22. Kim KH, Jung DW, Pham VH, Chung JS, Kong BS, Lee JK, Kim K, Oh ES (2012) Performance enhancement of Li-ion batteries by the addition of metal oxides (CuO, Co_3O_4)/solvothermally reduced graphene oxide composites. Electrochim Acta 69:358–363
23. Pham VH, Cuong TV, Hur SH, Oh ES, Kim EJ, Shin EW, Chung JS (2011) Chemical functionalization of graphene sheets by solvothermal reduction of a graphene oxide suspension in *N*-methyl-2-pyrrolidone. J Mater Chem 21:3371–3377

24. Zhao Y, Zhan L, Tian J, Nie S, Ning Z (2011) Enhanced electrocatalytic oxidation of methanol on Pd/polypyrrole—graphene in alkaline medium. Electrochim Acta 56:1967–1972
25. Ma HL, Qi XR, Maitani Y, Nagai T (2007) Preparation and characterization of superparamagnetic iron oxide nanoparticles stabilized by alginate. Int J Pharm 333:177–186
26. Kim K, Ahn S, Kim HS, Liu HK (2009) Electrochemical and thermal properties of 2,4,6-tris(trifluoromethyl)-1,3,5-triazine as a flame retardant additive in Li-ion batteries. Electrochim Acta 54:2259–2265
27. Yang S, Huo J, Song H, Chen X (2008) A comparative study of electrochemical properties of two kinds of carbon nanotubes as anode materials for lithium ion batteries. Electrochim Acta 53: 2238–2244